

1 **Using computer-aided image processing to estimate chemical**  
2 **composition of igneous rocks: A potential tool for large-scale**  
3 **compositional mapping**

4 Julin Zhang\*, Cin-Ty A. Lee, Michael Farner

5 *Department of Earth, Environmental and Planetary Sciences, Rice University,*  
6 *Houston, TX, United States*

7

8 \*Corresponding author

9 E-mail: zhangjulin89@gmail.com

10

11 **Abstract**

12 Digital cameras, particularly on smartphones, have led to the proliferation of amateur  
13 photographers. Of interest here is the use of smartphone cameras to conduct rapid,  
14 low-cost compositional mapping of geologic bedrock, such as plutons and batholiths,  
15 in combination with chemical analyses of rocks in the laboratory. This paper  
16 discusses some of the challenges in geochemical mapping using image analysis. We  
17 discuss methods for color calibration through a series of experiments under different  
18 light intensities and conditions (spectra). All indoor and outdoor experiments show  
19 good reproducibility, but suffer from biases imparted by different light intensities,  
20 light conditions, and camera exposure times. These biases can be greatly reduced with  
21 a linear color calibration method. Over-exposed and under-exposed images, however,  
22 cannot be fully calibrated, so we discuss methods that ensure images are properly  
23 exposed. We applied our method to 59 natural granitoid samples of known chemical  
24 composition. Strong correlations between average gray levels and major element  
25 compositions were observed, indicating that very subtle variations in bulk  
26 composition can potentially be rapidly assessed using calibrated photographs of  
27 outcrops.

28

29 Keywords: mapping; image processing; color calibration; geochemistry

## 30 **1. Introduction**

31           There is a growing need for rapid, large-scale compositional mapping of  
32 outcrops and land surface as the pressures for mineral exploration and environmental  
33 assessment grow. The most accurate approach for compositional mapping is to collect  
34 samples from the field and analyse them in the laboratory through various geo-  
35 analytical methods (X-ray fluorescence, inductively coupled plasma mass  
36 spectrometry, etc.), but these approaches are too expensive and too slow to fully  
37 support rapid, large-scale compositional mapping (Potts, 2012). There is thus a need  
38 to explore other methods that may be less precise but compensate for this deficiency  
39 by allowing for the accumulation of large datasets. The best trained geologists serve  
40 as walking image processors and analyzers as they are trained to identify rocks and  
41 interpret their origins from rock textures and colors based solely on the unaided eye  
42 and years of experience. Human eyes and brains are not the same, so considerable  
43 observer variability and bias is introduced when more than one geologist is  
44 conducting a lithological survey. Computer-aided processing of rock textures has thus  
45 become an important part of quantifying such quantities as grain size, shape and  
46 spatial distribution in igneous and metamorphic petrology (Åkesson et al., 2003;  
47 Cashman and Ferry, 1988; Cashman and Marsh, 1988; Heilbronner, 2000; Jerram et  
48 al., 2003; Kemeny et al., 1993).

49           In this paper, we explore the use of color in quantifying the composition of  
50 igneous rocks. Because color can correlate with mineralogy, it might be expected to  
51 correlate with composition for a certain range of geologic materials. There are,  
52 however, many challenges in using color quantitatively because many variables  
53 control color and its perception (Stevens et al., 2007). For example, alteration can  
54 easily modify the surface color of mineral grains. In addition, apparent color varies

55 depending on the spectrum of light, which can change throughout the day or under  
56 different lighting conditions (Foster, 2011; Romero et al., 2003). There is thus a need  
57 for robust color calibration, particularly if color is being assessed outdoors when  
58 conditions change continually. In the soil science community, eye-based side-by-side  
59 comparison with the Munsell color chart has been widely used to quantify soil color  
60 in the field (Color, 1998; Pendleton and Nickerson, 1951; Rossel et al., 2006). Similar  
61 computer-based calibration against color guides (Joshi and Jensen, 2004; Pascale,  
62 2006) has been applied to problems in food science, biosciences, agriculture and  
63 planetary exploration (Allender et al., 2018; Costa et al., 2010; Fischer, 2019; Wu and  
64 Sun, 2013).

65         Here, we develop a method for quantifying color from images taken from  
66 simple hand-held digital cameras or phone cameras, opening an opportunity for large-  
67 scale, high resolution mapping using citizen science. We note that the development of  
68 plant and animal identification algorithms in mobile phone apps has decreased the  
69 barriers for citizens to report observations, resulting in the largest and most  
70 comprehensive biodiversity survey of the planet to date, a feat that could never have  
71 been accomplished by all living scientists combined (Sullivan et al., 2014; Van Horn  
72 et al., 2018). Our long-term goal is to use color and texture-based image analysis to  
73 map out compositional variations of a pluton on the scale of meters or less. Our long  
74 term goals are to be able to use such compositional maps to better understand the  
75 dynamics of magmatic systems. This paper is a small step towards that goal. It is the  
76 hope that subtle variations in composition can be detected by quantifying subtle  
77 variations in color.

78

## 79 **2. Material and methods**

### 80 **2.1. Samples**

81 Image analyses were conducted on felsic granitoids from the Bernasconi Hills  
82 pluton, northern Peninsular Ranges Batholith in California, USA (Farner et al., 2017).  
83 The samples consist primarily of quartz and plagioclase with small amounts of  
84 hornblende and biotite. Felsic or silicic minerals, such as quartz and plagioclase,  
85 appear as transparent or white, whereas mafic minerals like hornblende and biotite are  
86 dark brown to black. Our goal was to quantify the “mafic index”, that is, the bulk gray  
87 level and relative proportions of dark minerals using image analysis, and in particular,  
88 to explore the challenges of quantifying mafic index under variable lighting  
89 conditions.

### 90 **2.2. Experimental setup**

91 We first conducted a series of indoor experiments under controlled light  
92 conditions to gain a sense of how ambient light affects perceived color. In all  
93 experiments, we used an iPhone 7 Plus digital camera with an aperture of f/1.8. For  
94 indoor lighting, we used two TaoTronics™ LED table lamps (12 W and 410 lumens).  
95 These LED table lamps have 5 lighting conditions (cold white - CW, white - W,  
96 natural - N, yellow -Y and warm yellow - WY) and 7 intensity levels where level 1  
97 refers to the lowest intensity and level 7 for highest intensity. The two LED lamps  
98 were placed 26 cm over the sample and with a separation distance between the two  
99 lamps of 23 cm to minimize shadows (Fig. 1(a)). The camera was placed slightly  
100 higher than the lamps to avoid generating shadows (Fig. 1(a)). A phone holder and  
101 camera shutter remote control were used to avoid vibrations.

102 In order to calibrate color, we placed a X-Rite ColorChecker Passport™,  
103 which has 24 pure color patches with known sRGB values, adjacent to the rock  
104 sample for all photographs (Fig. 1(b)). Instead of using the default camera application  
105 in the iPhone 7 Plus, which stores images in the form of JPEGs, photographs were  
106 taken using an App called Camera+™. Camera+™ stores images in DNG format,  
107 which is a raw file format that does not normalize the spectral histogram of an image.  
108 Camera+™ also allows the option to manually change camera settings, such as  
109 exposure time and ISO, etc. However, for indoor experiments, we used auto mode,  
110 which allows the program to automatically choose the proper exposure time and ISO.

111 Image experiments were also performed outdoors under natural daylight  
112 conditions. Due to the high intensity of daylight and the ease to which iPhone cameras  
113 become saturated, pictures taken with an iPhone under bright daylight are usually  
114 overexposed, making it difficult if not impossible to calibrate an overexposed image.  
115 To solve this problem, we attached a PolarPro™ Iris neutral density filter (ND filter)  
116 in front of the camera lens. We used the ND8 filter, which reduces the amount of  
117 incident light by a factor of 8 but does not change the spectrum of the incident light.  
118 Unlike the auto mode choice for indoor experiments, we manually set the exposure  
119 time and ISO for outdoor experiments and explored the effect of camera settings on  
120 the performance of the calibration.

### 121 ***2.3. Calibration method***

122 Because the colors of minerals in our rock samples are primarily black and  
123 white, we studied the gray level histogram of the images instead of three separated  
124 RGB histograms. The algorithm of converting RGB tristimulus values of a pixel in  
125 the sRGB color space to one gray level value used in this paper follows the ITU-R  
126 Recommendation BT.601(BT, n.d.):

127  $Gray = Red * 0.299 + Green * 0.587 + Blue * 0.114$  (1)

128 Luminosity calibration is usually required before color calibration to  
129 compensate for spatially heterogeneous transmission of light across the camera lens  
130 area (Hong et al., 2001; Losey, 2003). We used a white calibration board on the X-  
131 Rite ColorChecker Passport™ to check for spatial homogeneity of luminosity  
132 distribution by placing the white board in exactly the same positions where the sample  
133 and the color checker would sit. The same camera settings were adopted for all  
134 photographs (exposure time of 1/120 and ISO of 25). Our results show that the gray  
135 level histograms of the two areas (sample and color checker) were very similar, with  
136 mean grayscale values within 2% (Fig. 2(a,b)). There was thus no need to perform  
137 any luminosity calibrations before color calibrations. In the field, so long as the light  
138 source is diffuse on the length scale of the sample, luminosity corrections are not  
139 needed.

140 Color was calibrated with the X-Rite ColorChecker Passport™, which offers  
141 24 color patches with known sRGB values. RGB measurements of each of the 24  
142 color patches were mapped to the ‘real’ RGB tristimulus values to develop a  
143 calibration model for each photograph. A linear model shown below was assumed:

144  $Red_{calib} = \alpha_0 + \alpha_1 * Red + \alpha_2 * Green + \alpha_3 * Blue$   
145  $Green_{calib} = \beta_0 + \beta_1 * Red + \beta_2 * Green + \beta_3 * Blue$   
146  $Blue_{calib} = \gamma_0 + \gamma_1 * Red + \gamma_2 * Green + \gamma_3 * Blue$  (2)

147 where  $Red_{calib}$ ,  $Green_{calib}$  and  $Blue_{calib}$  refer to the red, green and blue values of a  
148 pixel in the rock image after calibration,  $Red$ ,  $Green$  and  $Blue$  represent the actual  
149 RGB values of the standard, and  $\alpha$ ,  $\beta$  and  $\gamma$  are the parameters of the model. These  
150 parameters are determined by least squares fitting of the data to the above model.

151 **2.4. Feature extraction from histograms**

152           The gray level histogram of the rock image is assumed to be a mixture of two  
153 signals, each of which represents the signal of a dark or light mineral group. These  
154 two signals can be segmented by Otsu thresholding algorithm (Otsu, 1979). The dark  
155 and light mineral proportions were then estimated based on the binarization result. In  
156 addition, the average gray level intensity of histograms, which evaluate the overall  
157 gray level intensity of the rock image, also was considered in this study. All the  
158 programs in this study were coded in Python 3.6 (code can be accessed via  
159 [https://github.com/Zhangjulin/Color\\_calibration/blob/master/Color\\_calibration.py](https://github.com/Zhangjulin/Color_calibration/blob/master/Color_calibration.py)).

160

### 161 **3. Results**

#### 162 *3.1. Reproducibility of indoor and outdoor experiments*

163           In order to evaluate internal reproducibility, images of a same rock sample  
164 along with the color checker (Fig. 1(b)) were taken 10 times under the same light  
165 condition. We checked the consistency of gray level histograms among these 10  
166 images before and after color calibration. The reproducibility experiments were done  
167 both indoor and outdoor. For the indoor reproducibility experiments, two LED lamps  
168 were set to white (W) light condition and intensity level of 5. Auto mode on the  
169 iPhone was used, resulting in an exposure time of 1/300 and ISO of 25. For the  
170 outdoor reproducibility experiments under daylight, we attached a ND8 filter to the  
171 iPhone camera to avoid overexposure and we manually set the exposure time to 1/750  
172 and ISO to 25.

173           The results show that both indoor and outdoor histograms have good internal  
174 consistency before and after color calibration (Fig. 3). We note that there is a small  
175 spike at gray level intensity of 0 in the outdoor non-calibrated histograms (Fig. 3(c)),  
176 indicating a slight underexposure. In any case, histograms are bimodal with the left



177 peak representing the dark mineral mode and the right peak representing the light  
178 mineral mode. These two modes overlap between gray level intensity 60 to 130.

179 Average gray level intensities and mineral proportions were later determined  
180 from calibrated histograms. We also evaluated reproducibility of these two indices.  
181 The results show that the mean value of dark mineral proportion for indoor  
182 experiments is 0.365 with a relative two standard deviation (2RSD) of 1.54% while  
183 the mean and 2RSD for outdoor experiments are 0.354 and 0.680% (detailed data can  
184 be found in the supplemental materials). The mean and 2RSD of dark mineral  
185 proportion between indoor and outdoor experiments were similar. The average gray  
186 level for indoor experiments is 125.2 (2RSD = 0.12%) and 117.2 (2RSD = 0.22%) for  
187 outdoor experiments.

### 188 ***3.2. Indoor experiments***

189 We accumulated 35 images of a same granitoid sample (Fig. 1(b)) indoors  
190 with different LED light conditions or intensities. The gray level histograms of these  
191 35 images after color calibration show more internal consistency than before color  
192 calibration (Fig. 4). The discrepancy of uncalibrated histograms comes from the  
193 difference in LED light conditions and intensities.

194 We first checked the RGB measurements of the color checker to see how light  
195 intensity biases color. Fig. 5 shows measured versus actual color for the color checker  
196 under CW, W, N, Y and WY light conditions with intensity levels of 1, 5 and 7. Every  
197 data point in Fig. 5 represents red (green or blue) measurements corresponding to the  
198 24 calibration standards. Deviations from the 1:1 line indicate measurement bias. All  
199 experiments show some level of bias. For Y and WY light conditions, the degree of  
200 bias appears to be independent of intensity level (Fig. 5(j-o)). This is because the  
201 iPhone auto exposure program adequately changes exposure time and ISO to

202 compensate for different light intensity. Bias remains constant for CW, W, and N light  
203 conditions when intensity increases from level 1 to level 5 (Fig. 5(a,b,d,e,g,h)), but  
204 when intensity increases to level 7, there is an increase in the negative deviation of  
205 measured values compared to standard values (Fig. 5(c,f,i)).

206         Of particular interest is how the degree of bias varies between different light  
207 conditions, which would indicate that the spectrum of light influences color  
208 perception. For an intensity level of 5 (Fig. 5(b,e,h,k,n)), measurements under CW, W  
209 and N mostly fall close to the 1:1 line (Fig. 5(b,e,h)), with the exception of  
210 measurements lower than 100, which fall below the 1:1 line. We also note that the  
211 blue data are systematically higher than the green and red data. When Y light is used,  
212 some blue data go to zero, indicating underexposure (Fig. 5(k)). Unlike CW, W and N  
213 light conditions, the red data under Y light conditions are systematically higher than  
214 the green and blue data. For WY light, red, green and blue data all show significant  
215 bias from the standard (Fig. 5(n)) although the data parallel the 1:1 line.

216         The color biases observed for the different light conditions are undoubtedly  
217 due to differences in the spectrum of the 5 light conditions. CW and W light have  
218 more short wavelength light (blue) but less long wavelength light (red), so the  
219 reflected light of the color checker will have more blue than red light (Fig. 5(b,e)). In  
220 contrast, Y and WY light have more long wavelength light than short wavelength  
221 light, and as a consequence, the reflected light has more red than blue light (Fig.  
222 5(k,n)).

223         The above experiments were also used to explore the effects of light intensity  
224 and light condition (spectrum) on gray level histograms (Fig. 6-7). Uncalibrated  
225 histograms regardless of light condition are consistent between light intensities of 1-5  
226 (Fig. 6(a,c-f)), but shift darker at intensity level of 6 and 7 for CW, W and N light

227 conditions (Fig. 6(a,c,d)). However, after calibration, histograms converge and are  
228 consistent across all light intensities (Fig. 6(b)). The calibrated histograms become  
229 slightly compressed compared to the uncalibrated histograms (Fig. 6(a,b)).

230 The effects of light condition on gray level histograms were also explored.  
231 Fig. 7(a,c,e) show the comparisons of uncalibrated gray level histograms for different  
232 light conditions under the same light intensity level (1, 4 and 7). Varying light  
233 condition caused the centroid of dark and light minerals to migrate. In particular, the  
234 light mineral mode in WY light becomes compressed and shifts darker compared to  
235 other light conditions, although this effect diminishes when light intensity increases to  
236 7 (Fig. 7(e)). After calibration, histograms in WY light converge to that of other light  
237 conditions (Fig. 7(b,d,f)).

238 Average gray level and mineral proportions were estimated from both  
239 uncalibrated and calibrated histograms. The mean value of average gray level of  
240 uncalibrated histograms is 115.0 (2RSD = 6.2%) and that of calibrated histograms is  
241 125.3 (2RSD = 0.78%). The mean value of calibrated results is ~9% larger than for  
242 the uncalibrated results, and the variance of calibrated results is much smaller. The  
243 mean value of the dark mineral proportion estimated from uncalibrated histograms is  
244 0.359 (2RSD = 2.68%), and 0.360 (2RSD = 2.80%) for calibrated histograms. The  
245 mineral proportion estimated from uncalibrated and calibrated histograms are similar.  
246 While mean grayscale and mineral proportion values are similar for different lighting  
247 conditions, there is more variation in the magnitude of the 2RSDs across light  
248 conditions (Table 1). CW light displays the largest variability whereas WY light  
249 displays the smallest variability, with 2RSD decreasing as the softness of light  
250 increases.

### 251 ***3.3. Outdoor experiments under uncontrolled daylight***

252 In order to study the influence of dynamic daylight in gray level histograms,  
253 we conducted 20 series of outdoor experiments at different times of the day (from  
254 morning to afternoon) and on days with different lighting conditions (sunny and  
255 cloudy days).

256 Here, we present the results of one representative outdoor experiment  
257 performed on a sunny afternoon. We first explored auto mode (exposure time of  
258  $\sim 1/3500$  and ISO of 20). Nearly all RGB measurements of the color checker deviate  
259 positively from the standard values (Fig. 8(a)). Some RGB measurements even  
260 approach the saturation limit (255), which indicates overexposure. The uncalibrated  
261 histogram under auto mode shifts much lighter compared to indoor uncalibrated  
262 histograms as exemplified in Fig. 8(b) for N light condition and intensity level of 4.  
263 A linear color calibration was found to fix the shift but there remains obvious  
264 discrepancy between the histogram shape, especially towards the dark mineral mode  
265 (Fig. 8(c)).

266 To improve on this, we attached a ND8 filter to the iPhone 7 Plus, which  
267 reduces the amount of light transmitted to the camera. Images were taken with a series  
268 of different exposure times (1/500, 1/750, 1/1000 and 1/1500) with ISO manually  
269 fixed to 25 to be consistent with the indoor experiments. The exposure time of 1/500  
270 combined with a ND8 filter still results in overexposure and does not improve results  
271 (Fig. 8(d-f)). When the exposure time decreases to 1/750 and 1/1000, the discrepancy  
272 between measurements and standards in the color checker are reduced, and both the  
273 uncalibrated and calibrated histograms match better with reference histograms (Fig.  
274 8(g-l)). However, when exposure time decreases to 1/1500, all the RGB  
275 measurements fall below the corresponding standards due to underexposure (Fig.  
276 8(m)). This underexposure drives the uncalibrated histogram to shift darker (Fig. 8(n))

277 and worsens the calibrated histogram (Fig. 8(o)). These results show that a too small  
278 or too large exposure time will distort the histogram even after calibration. Therefore,  
279 an optimal exposure time window is necessary, and for this outdoor experiment,  
280 exposure time of 1/750-1/1000 is favored.

281         The results of other 19 outdoor experiments show that the optimal exposure  
282 time varies under different daylight conditions (see supplemental data). Average gray  
283 levels and dark mineral proportions of there 20 outdoor experiments were determined  
284 from calibrated histograms that are properly exposed. The mean value of average gray  
285 levels for these 20 experiments is 115.5 (2RSD = 4.3%, Table 2). The outdoor mean  
286 value is ~8% lower than the indoor result (125.3, 2RSD = 0.78%) and has a larger  
287 2RSD. The mean value of dark mineral proportions is 0.365 (2RSD = 8.07%), which  
288 is close to the indoor result (0.360, 2RSD = 2.80%) but has a larger 2RSD. Without  
289 the assistance of a ND filter, both the average gray level (115.9, 2RSD = 6.0%) and  
290 mineral proportion estimates (0.339, 2RSD = 18.6%) exhibit much larger variation  
291 (Table 2).

292

## 293 **4. Discussion**

### 294 ***4.1. Prospects and pitfalls of indoor imaging***

295         The reproducibility tests show that an iPhone 7 Plus, combined with Camera+  
296 APP, is able to obtain consistent gray level histograms under the same light condition  
297 (Fig. 3(a,c)). The linear color calibration method maintains this consistency even  
298 though histogram shapes are changed (Fig. 3(b,d)). Limited variation of average gray  
299 level and dark mineral proportions estimated from calibrated histograms indicate that  
300 our method is robust.

301 Indoor experiments show that varying light conditions impacts color  
302 information (Fig. 5). Differences in light conditions or intensity can lead to  
303 inconsistency of gray level histograms on the same rock sample (Fig. 6(a,c-f) and Fig.  
304 7(a,c,e)). However, we showed that consistency can be improved significantly with a  
305 linear calibration (Fig. 6(b) and Fig. 7(b,d,f)), supporting the validity of our method to  
306 calibrate histograms under indoor conditions.

#### 307 ***4.2. Prospects and pitfalls of outdoor imaging***

308 Outdoor experiment results show that auto mode is very likely to overexpose  
309 images (Fig. 8(a,b)). We also show that a linear calibration cannot perfectly calibrate  
310 the histograms (Fig. 8(c)). Therefore, for field geological mapping, it is wise to use  
311 manual mode with a ND filter and set proper exposure time appropriate to the  
312 daylight condition (Fig. 8(d-o)). However, it is difficult to determine the optimal  
313 exposure time if an indoor reference is not known, which would likely be the case for  
314 the casual citizen scientist. One way to solve this problem is to check the  
315 measurement-standard diagram of the color checker to see whether all the data lies  
316 around the 1:1 line, but this approach may be too qualitative.

317 Here, we explore a more quantitative method to determine the optimal  
318 exposure time window under arbitrary daylight conditions without knowledge of an  
319 indoor reference. Based on the consistency between indoor and outdoor histograms,  
320 we categorized all 90 images from 20 outdoor experiments into three groups: proper  
321 exposed images, underexposed images, and overexposed images. These three groups  
322 can be well classified by the red channel measurement of the orange patch ('I' in Fig.  
323 9(a)) and blue patch ('II' in Fig. 9(a)) of the color checker since the red channels of  
324 these two colors are sensitive to the light intensity change (Fig. 9(b)). The blue, red  
325 and black data symbols in Fig. 9(b) represent the overexposed, proper exposed and

326 underexposed data, respectively. Under proper exposure, data fall in a window  
327 bounded by the overexposed and underexposed data (Fig. 9(b)): 225-240 for the  
328 orange patch and 10-30 for the blue patch. For other brand color checkers, the optimal  
329 window for those two patches may be different and needs to be studied.

### 330 ***4.3. Estimating dark and light mineral proportions***

331 Average gray level and dark mineral proportion were determined from the  
332 histograms. Overall, these two indexes of indoor experiments vary much smaller than  
333 outdoor experiments (Table 2). This may due to the uncontrolled property of daylight.  
334 Indoor experiment results show that the average gray level of calibrated histograms  
335 has much smaller variation (2RSD = 0.78%) than uncalibrated histograms (2RSD =  
336 6.2%). This means that calibration can greatly improve the consistency of average  
337 gray level under different light conditions. The dark mineral proportion results  
338 between calibrated and uncalibrated histograms are similar. This is because within the  
339 variability of indoor light conditions, calibration does not significantly change the  
340 shapes of the histograms which determine the Otsu thresholding results. In contrast,  
341 for the outdoor experiments without ND filter, calibration significantly changes the  
342 shapes of histograms (Fig. 8(c)). Therefore, the dark mineral proportion results  
343 (0.339, 2RSD = 18.6%) are not consistent well with the indoor experiments (0.360,  
344 2RSD = 2.80%, Table 2). The much better result of proper exposed outdoor  
345 experiments with a ND filter (0.365, 2RSD = 8.07%, Table 2) supports the necessity  
346 of ND filter under daylight condition.

### 347 ***4.4. Application to petrology***

348 The calibration method proposed in this paper can provide precise and  
349 consistent histograms, which store valuable color information, of rock samples under

350 different light conditions. Some features, such as average gray level, of the histograms  
351 may correlate with chemical components of rocks considering the association between  
352 color information and mineralogy. To test this hypothesis, we did indoor experiments  
353 on 59 rock samples for which bulk chemical compositions were analyzed by XRF.  
354 These rocks are from the Bernasconi Hills pluton in the northern Peninsular Ranges  
355 Batholith in California, USA(Farner et al., 2017). Thirty-five of these samples are  
356 felsic granitoids and the remaining are mafic enclaves. Only the fresh faces of rock  
357 samples were used here since weathering can cause discoloration of mineral surfaces.  
358 We followed our indoor protocols outlined above. Rock samples were placed under  
359 two LED lamps along with a color checker for color calibration. All the 59  
360 experiments were carried out under N light condition and light intensity level of 4.

361         The results show that the average gray levels of calibrated histograms  
362 correlate well with some chemical components (Fig. 10). Gray scale correlates  
363 negatively with FeO, MnO and MgO, and positively with SiO<sub>2</sub>, which we attribute to  
364 the fact that the most abundant dark mineral in these samples is hornblende, which is  
365 rich in Fe, Mn and Mg. For FeO and MnO, the R<sup>2</sup> of correlations can reach 0.9 (Fig.  
366 10(a,b)), and for MgO and SiO<sub>2</sub> are above 0.85 (Fig. 10(c,d)). Given the fact that  
367 outdoor 2RSD result of average gray level is ~4.3% (Table 2), these correlations from  
368 indoor experiments imply that our method may also work for outdoor compositional  
369 mapping. In this paper, we only explored the correlation between average gray level  
370 and chemical composition. Some mining industry studies show that the correlation  
371 can be improved further if more color features or even textural features are  
372 incorporated (Bonifazi et al., 2001; Haavisto et al., 2006; Hargrave and Hall, 1997;  
373 Hargrave et al., 1996; Oestreich et al., 1995). Therefore, a more generalizable model



374 can be developed as more features and data are accumulated, serving potentially as a  
375 powerful tool to predict the chemical compositions of rock by image analysis.

376         There are of course some limitations in our method. In this paper, we focus on  
377 the gray level histograms because our rock samples only have dark and light minerals.  
378 For rocks containing more ‘colorful’ minerals, it will be better to study the three RGB  
379 histograms separately or even to consider the HSI color space. However, this paper is  
380 a step towards this direction of full color image analysis. In the future, we hope to  
381 explore other features, such as peak amplitude, peak width, etc.

382

### 383 **5. Conclusions**

384         In this paper, we proposed a simple but detailed method for imaging and color  
385 calibration of rocks using a digital camera on an iPhone 7 Plus. This simple color  
386 calibration method, assisted with a color checker as standard, can greatly improve the  
387 consistency of gray level histograms of the rock sample under different light  
388 conditions. We also showed that average gray levels of calibrated histograms strongly  
389 correlate with some chemical contents of 59 plutonic rocks, indicating that our  
390 method has potential for being an efficient tool for compositional mapping at large  
391 scale.

392

393 **Acknowledgements**

394 We thank Luca Giancardo for his generous advice on image processing. We thank  
395 Ming Tang and Wenrong Cao for discussions. This work was supported by the U.S.  
396 NSF via EAR- 1753599.

397

398 **Disclosure statement**

399 No potential conflict of interest was reported by the authors.

400

401 **References**

- 402 Allender, E.J., Stabbins, R.B., Gunn, M.D., Cousins, C.R., Coates, A.J., 2018. The  
403 ExoMars Spectral Tool (ExoSpec): an image analysis tool for ExoMars 2020  
404 PanCam imagery, in: Presented at the Image and Signal Processing for Remote  
405 Sensing XXIV, International Society for Optics and Photonics, p. 107890I.
- 406 Åkesson, U., Stigh, J., Lindqvist, J.E., Göransson, M., 2003. The influence of  
407 foliation on the fragility of granitic rocks, image analysis and quantitative  
408 microscopy. *Engineering Geology* 275–288.
- 409 Bonifazi, G., Serranti, S., Volpe, F., Zuco, R., 2001. Characterisation of flotation froth  
410 colour and structure by machine vision. *Computers & Geosciences* 27, 1111–  
411 1117.
- 412 BT, R.I.-R., n.d. Studio encoding parameters of digital television for standard 4: 3 and  
413 wide-screen 16: 9 aspect ratios.
- 414 Cashman, K.V., Ferry, J.M., 1988. Crystal size distribution (CSD) in rocks and the  
415 kinetics and dynamics of crystallization. *Contributions to Mineralogy and  
416 Petrology* 99, 401–415.
- 417 Cashman, K.V., Marsh, B.D., 1988. Crystal size distribution (CSD) in rocks and the  
418 kinetics and dynamics of crystallization II: Makaopuhi lava lake. *Contributions to  
419 Mineralogy and Petrology* 99, 292–305.
- 420 Color, M., 1998. Munsell soil color charts. Munsell Color.
- 421 Costa, C., Pallottino, F., Angelini, C., Proietti, M., Capoccioni, F., Aguzzi, J.,  
422 Antonucci, F., Menessati, P., 2010. Colour calibration for quantitative biological  
423 analysis: A novel automated multivariate approach. *Instrumentation viewpoint  
424* 70–71.
- 425 Farner, M.J., Lee, C.-T.A., Mikus, M.L., 2017. Geochemical signals of mafic-felsic  
426 mixing: Case study of enclave swarms in the Bernasconi Hills pluton, California.  
427 *GSA Bulletin* 130, 649–660. doi:10.1130/B31760.1
- 428 Fischer, T., 2019. PCA-based supervised identification of biological soil crusts in  
429 multispectral images. *MethodsX* 6, 764–772.
- 430 Foster, D.H., 2011. Color constancy. *Vision research* 51, 674–700.
- 431 Haavisto, O., Kaartinen, J., Hyotyniemi, H., 2006. Optical spectrum based estimation  
432 of grades in mineral flotation, in: Presented at the 2006 IEEE International  
433 Conference on Industrial Technology, IEEE, pp. 2529–2534.

434 Hargrave, J.M., Hall, S.T., 1997. Diagnosis of concentrate grade and mass flowrate in  
435 tin flotation from colour and surface texture analysis. *Minerals Engineering* 10,  
436 613–621.

437 Hargrave, J.M., Miles, N.J., Hall, S.T., 1996. The use of grey level measurement in  
438 predicting coal flotation performance. *Minerals Engineering* 9, 667–674.

439 Heilbronner, R., 2000. Automatic grain boundary detection and grain size analysis  
440 using polarization micrographs or orientation images. *Journal of Structural*  
441 *Geology* 22, 969–981.

442 Hong, G., Luo, M.R., Rhodes, P.A., 2001. A study of digital camera colorimetric  
443 characterization based on polynomial modeling. *Color Research & Application:*  
444 *Endorsed by Inter-Society Color Council, The Colour Group (Great Britain),*  
445 *Canadian Society for Color, Color Science Association of Japan, Dutch Society*  
446 *for the Study of Color, The Swedish Colour Centre Foundation, Colour Society of*  
447 *Australia, Centre Français de la Couleur* 26, 76–84.

448 Jerram, D.A., Cheadle, M.J., Philpotts, A.R., 2003. Quantifying the building blocks of  
449 igneous rocks: are clustered crystal frameworks the foundation? *Journal of*  
450 *Petrology* 44, 2033–2051.

451 Joshi, N., Jensen, H.W., 2004. Color calibration for arrays of inexpensive image  
452 sensors. Master's with Distinction in Research Report, Stanford University,  
453 Department of Computer Science 30.

454 Kemeny, J.M., Devgan, A., Hagaman, R.M., Wu, X., 1993. Analysis of rock  
455 fragmentation using digital image processing. *Journal of Geotechnical*  
456 *Engineering* 119, 1144–1160.

457 Losey, G.S., Jr, 2003. Crypsis and communication functions of UV-visible coloration  
458 in two coral reef damselfish, *Dascyllus aruanus* and *D. reticulatus*. *Animal*  
459 *Behaviour* 66, 299–307.

460 Oestreich, J.M., Tolley, W.K., Rice, D.A., 1995. The development of a color sensor  
461 system to measure mineral compositions. *Minerals Engineering* 8, 31–39.

462 Otsu, N., 1979. A threshold selection method from gray-level histograms. *IEEE*  
463 *transactions on systems, man, and cybernetics* 9, 62–66.

464 Pascale, D., 2006. RGB coordinates of the Macbeth ColorChecker. *The BabelColor*  
465 *Company* 6.

466 Pendleton, R.L., Nickerson, D., 1951. Soil colors and special Munsell soil color  
467 charts. *Soil Science* 71, 35–44.

468 Potts, P.J., 2012. A handbook of silicate rock analysis. Springer Science & Business  
469 Media.

470 Romero, J., Hernández Andrés, J., Nieves, J.L., García, J.A., 2003. Color coordinates  
471 of objects with daylight changes. *Color Research & Application: Endorsed by*  
472 *Inter-Society Color Council, The Colour Group (Great Britain), Canadian Society*  
473 *for Color, Color Science Association of Japan, Dutch Society for the Study of*  
474 *Color, The Swedish Colour Centre Foundation, Colour Society of Australia,*  
475 *Centre Français de la Couleur* 28, 25–35.

476 Rossel, R.V., Minasny, B., Roudier, P., McBratney, AB, 2006. Colour space models  
477 for soil science. *Geoderma* 133, 320–337.

478 Stevens, M., Párraga, C.A., Cuthill, I.C., Partridge, J.C., Troscianko, T.S., 2007.  
479 Using digital photography to study animal coloration. *Biological Journal of the*  
480 *Linnean society* 90, 211–237.

481 Sullivan, B.L., Aycrigg, J.L., Barry, J.H., Bonney, R.E., Bruns, N., Cooper, C.B.,  
482 Damoulas, T., Dhondt, A.A., Dietterich, T., Farnsworth, A., 2014. The eBird  
483 enterprise: an integrated approach to development and application of citizen  
484 science. *Biological Conservation* 169, 31–40.

485 Van Horn, G., Mac Aodha, O., Song, Y., Cui, Y., Sun, C., Shepard, A., Adam, H.,  
486 Perona, P., Belongie, S., 2018. The inaturalist species classification and detection  
487 dataset, in: *Presented at the Proceedings of the IEEE conference on computer*  
488 *vision and pattern recognition*, pp. 8769–8778.

489 Wu, D., Sun, D.-W., 2013. Colour measurements by computer vision for food quality  
490 control—A review. *Trends in Food Science & Technology* 29, 5–20.

491

492 **Tables**

493 Table 1. Average gray levels and dark mineral proportions estimated from calibrated

494 histograms under different light conditions

<i>Light condition</i>	<i>Average gray level</i>		<i>Dark mineral proportion</i>	
	<i>Mean</i>	<i>2RSD</i>	<i>Mean</i>	<i>2RSD</i>
<i>Cold white (CW)</i>	125.2	0.59%	0.357	3.95%
<i>White (W)</i>	125.4	0.42%	0.358	1.81%
<i>Natural light (N)</i>	125.6	0.27%	0.357	1.29%
<i>Yellow (Y)</i>	125.7	0.16%	0.359	1.75%
<i>Warm yellow (WY)</i>	124.5	0.18%	0.366	0.491%
<i>All</i>	125.3	0.78%	0.360	2.80%

495

496 Table 2. Average gray levels and dark mineral proportions estimated from calibrated  
 497 histograms indoors and outdoors

498

<i>Light condition</i>	<i>ND filter</i>	<i>Average gray level</i>		<i>Dark mineral proportion</i>	
		<i>Mean</i>	<i>2RSD</i>	<i>Mean</i>	<i>2RSD</i>
<i>Indoor</i>	No	125.3	0.78%	0.360	2.80%
<i>Outdoor</i>	Yes	115.5	4.3%	0.365	8.07%
<i>Outdoor</i>	No	115.9	6.0%	0.339	18.6%

499

500 **Figure legends**

501 **Figure 1. Indoor experiment environment and materials used in this project. (a)**

502 Two LED lamps were placed in parallel over the sample. An iPhone was placed  
503 above the lamps. (b) A granitoid sample, along with a color checker, was placed  
504 under the lamps.

505

506 **Figure 2. Results of luminosity experiments. (a)** Comparison of two gray level  
507 histograms of the same white board placed at the positions where the sample (orange  
508 histogram) and the color checker (blue histogram) should sit. (b) Zoomed in view of

509 (a). Gray level mean for sample and color checker locations are ~185 and ~190,  
510 respectively.

511

512 **Figure 3. Results of reproducibility experiments. (a)** Indoor result before  
513 calibration, (b) indoor result after calibration, (c) outdoor result before calibration and  
514 (d) outdoor result after calibration. Each panel shows the results of 10 independent  
515 experiments.

516

517 **Figure 4. Gray level histograms of the same granitoid sample under different**  
518 **indoor LED light conditions and intensities. (a)** Histograms before color calibration  
519 and (b) histograms after color calibration.

520

521 **Figure 5. Measurement of color-checker standards under different indoor light**  
522 **conditions and intensities.** X-axis represents standard values and Y-axis represents  
523 measured gray level. Color (red, green and blue) of each data point refers to the RGB  
524 tristimulus value of a particular color patch on the color checker. (a)-(c) CW light ,



525 (d)-(f) W light, (g)-(i) N light (j)-(l) Y light, and (m)-(o) WY light. Light intensity was  
526 fixed to level 1, 5 and 7 (columns).

527

528 **Figure 6. Gray level histograms of granitoid sample under constant indoor light**  
529 **conditions but different intensities.** (a) Uncalibrated and (b) calibrated histograms  
530 under CW light condition with different light intensity levels. Uncalibrated  
531 histograms under (c) W , (d) N , (e) Y , and (f) WY light with different light intensity  
532 levels.

533

534 **Figure 7. Gray level histograms of the granitoid sample under constant indoor**  
535 **light intensity but different light conditions.** (a) Uncalibrated and (b) calibrated  
536 histograms under different light conditions with light intensity fixed to level 1. (c)  
537 Uncalibrated and (d) calibrated histograms under different light conditions with light  
538 intensity fixed to level 4. (e) Uncalibrated and (f) calibrated histograms under  
539 different light conditions with light intensity fixed to level 7.

540

541 **Figure 8. Outdoor color calibration results with different exposure times.** (a)  
542 Comparison of measured gray scale to standard values of the color checker, (b)  
543 uncalibrated and (c) calibrated histograms of the granitoid sample when using auto  
544 exposure. The results when manually setting the exposure time to (d)-(f) 1/500, (g)-  
545 (i) 1/750, (j)-(l) 1/1000 and (m)-(o) 1/1500 seconds.

546

547 **Figure 9. A quantitative method to determine the optimal exposure time window**  
548 **under arbitrary daylight conditions.** (a) Orange and blue patches in the color  
549 checker were analyzed. (b) Red channel measurements of orange and blue patch for

550 20 outdoor experiments with different exposure times. The blue, red and black data  
551 points represent overexposed, properly exposed and underexposed data, respectively.

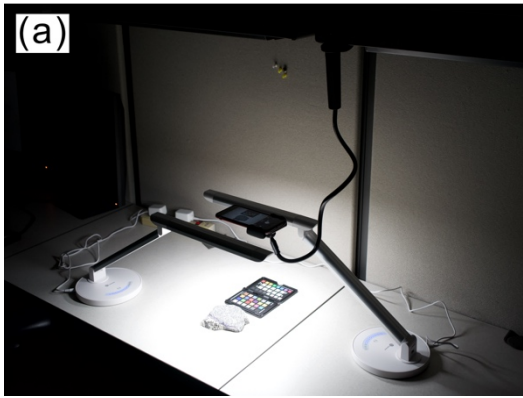
552

553 **Figure 10. Correlations between average gray level of calibrated histograms and**  
554 **major element contents from 59 rock samples.** Gray scale correlates negatively  
555 with whole-rock (a) FeO, (b) MnO and (c) MgO, and positively with (d) SiO<sub>2</sub> (wt. %).

556

557

Fig.1



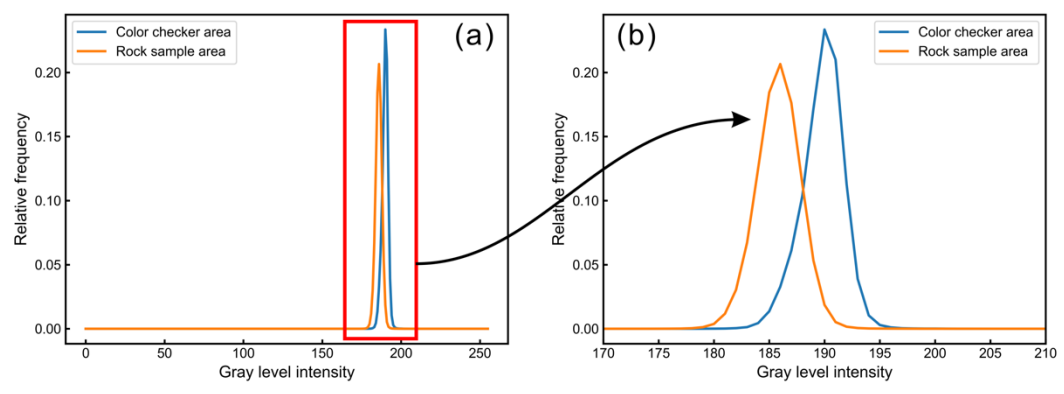
558



559

560

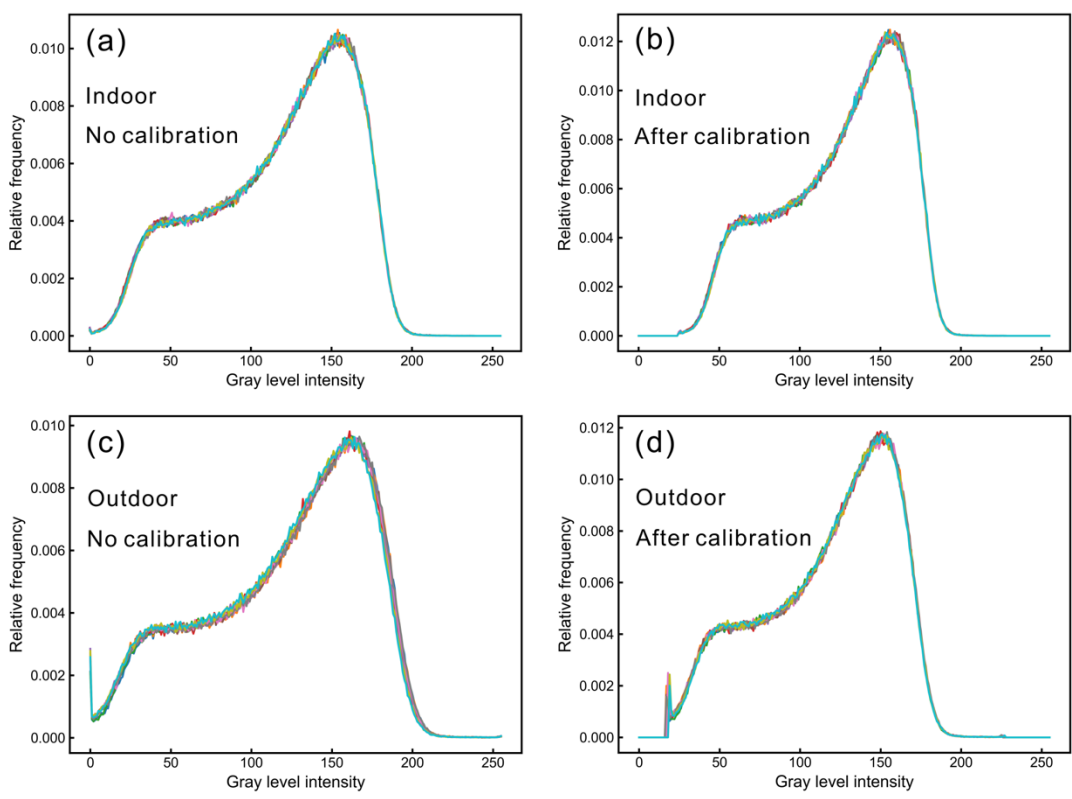
Fig.2



561

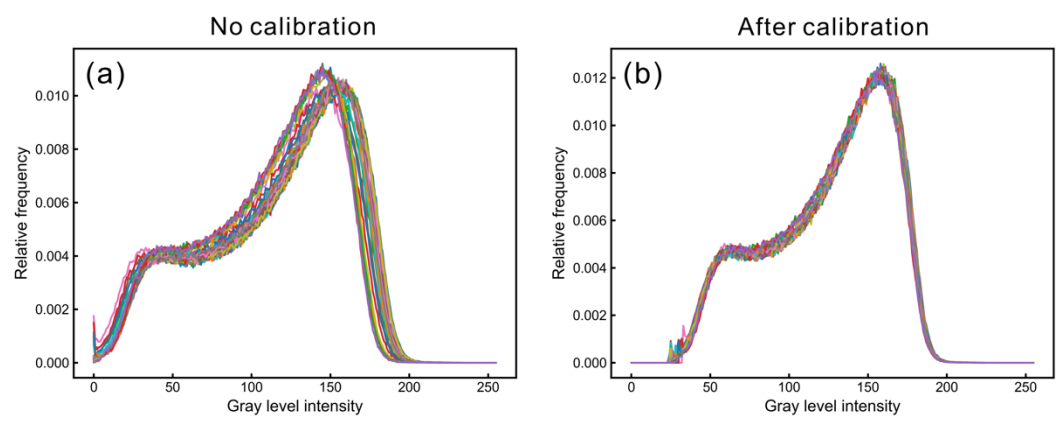
562

Fig.3



566

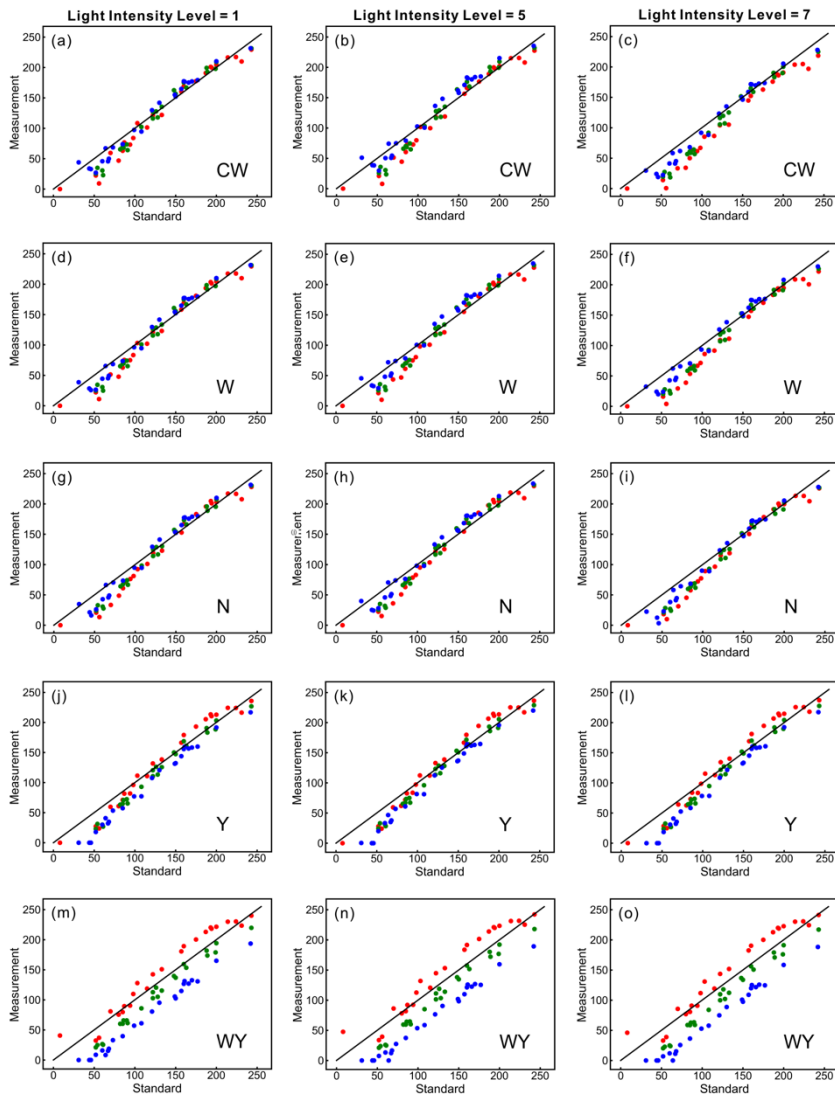
Fig.4



567

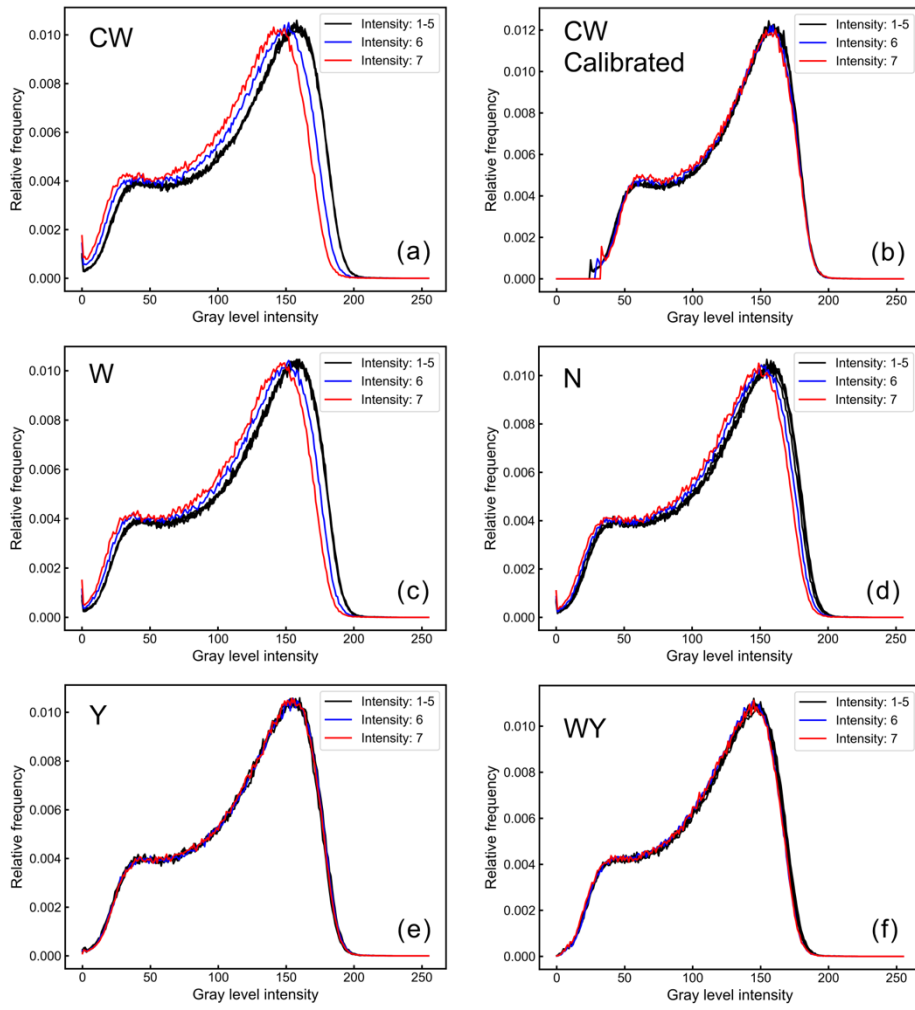
568

Fig.5



570

571





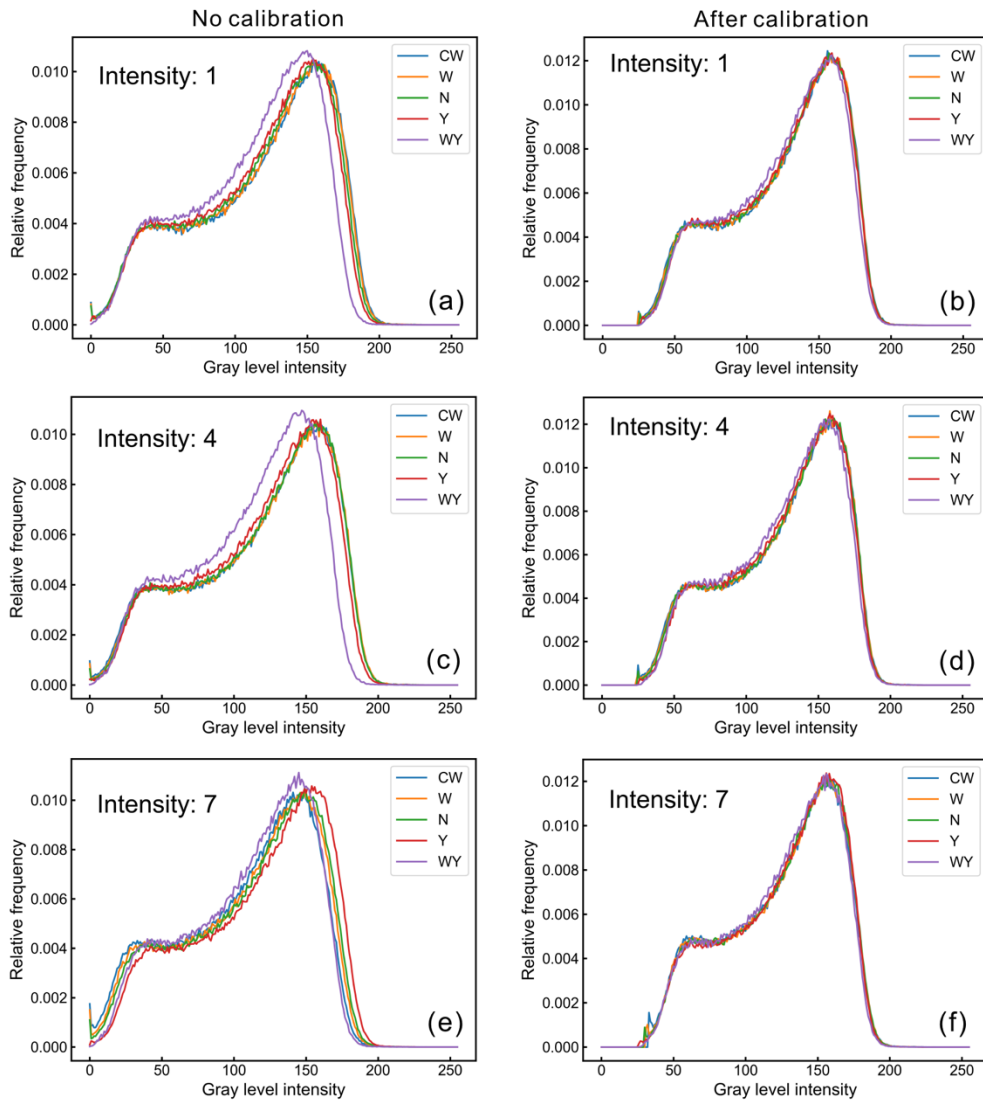


Fig.8

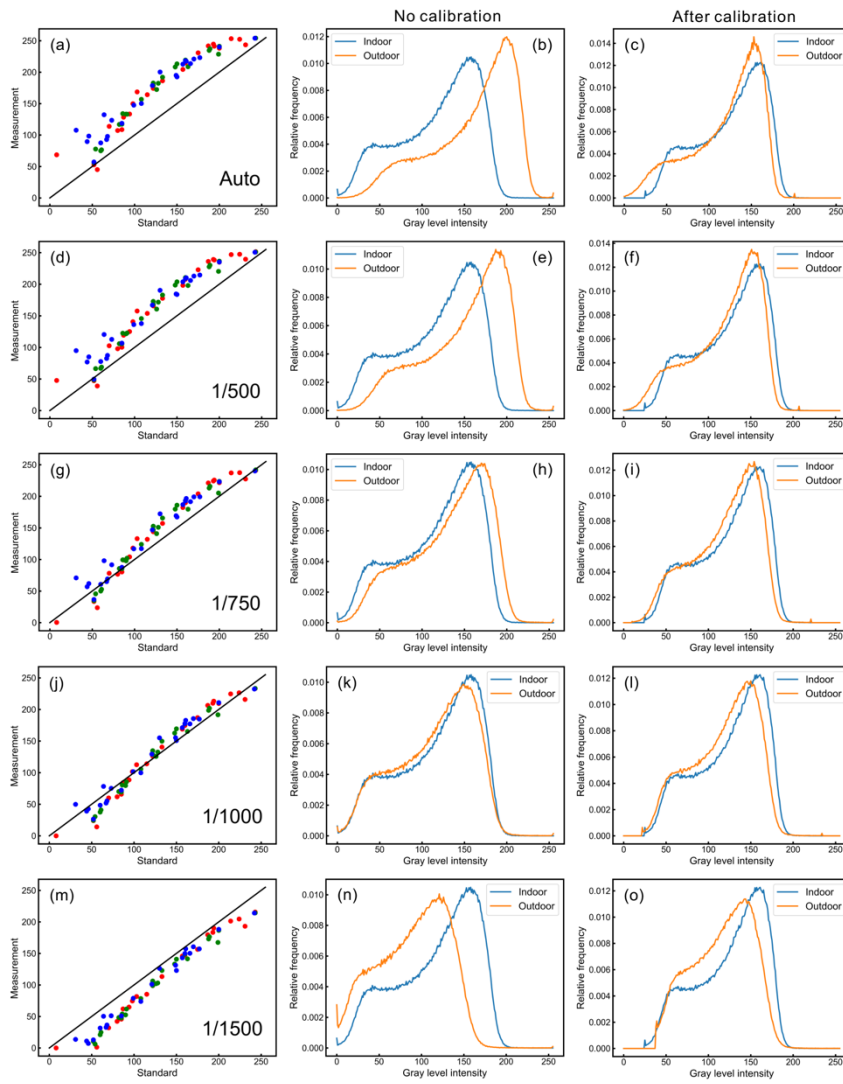


Fig.9

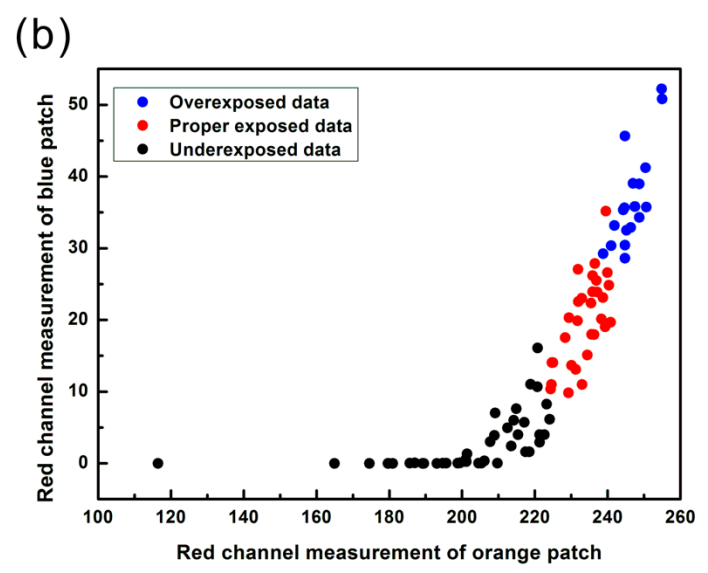


Fig.10

